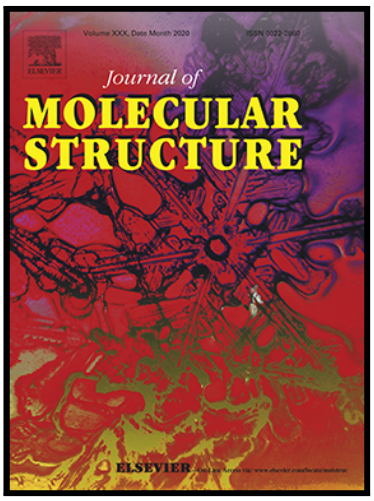

Study of antimicrobial and antioxidant activities of pyrrole-chalcones

Poonam Rawat , R.N. Singh , Alok Ranjan , Anshu Gautam , Sweta Trivedi , Mukesh Kumar

PII: S0022-2860(20)31798-1
DOI: https://doi.org/10.1016/j.molstruc.2020.129483
Reference: MOLSTR 129483

To appear in: *Journal of Molecular Structure*

Received date: 29 March 2020
Revised date: 20 September 2020
Accepted date: 17 October 2020

Please cite this article as: Poonam Rawat , R.N. Singh , Alok Ranjan , Anshu Gautam , Sweta Trivedi , Mukesh Kumar , Study of antimicrobial and antioxidant activities of pyrrole-chalcones, *Journal of Molecular Structure* (2020), doi: https://doi.org/10.1016/j.molstruc.2020.129483

Highlights

- All pyrrole-chalcones showed π→π* electronic excitations.
- Compound (**3a**, **3c**, **3g**, **3h**, **3i** and **5a**) displayed better NLO responses than standard p-NA.
- Studied compounds (**3a**, **3c**, **3g**, **3h**, **3i** and **5a**) have good antifungal and antibacterial activity.
- Studied compounds showed promising free radical scavenging and Fe^{+2} ion chelating activity.

Study of antimicrobial and antioxidant activities of pyrrole-chalcones

Poonam Rawat, R. N. Singh*, Alok Ranjan, Anshu Gautam, Sweta Trivedi, Mukesh Kumar

Department of Chemistry, University of Lucknow, Lucknow–226007, U.P., India

Abstract

The resistance of pathogenic microorganisms to accessible antibiotics, anxiolytics, sedatives, hypnotics and anti-convalsunts are rapidly forming a foremost problem worldwide. The detailed spectroscopic, DFT, antimicrobial, and antioxidant analysis of synthesized pyrrole chalcone derivatives (**3a**, **3c**, **3h**, **3i**, and **5a)** have been performed and interpreted. Occurring of doublet in ^{1}H NMR spectra of (**3a**, **3c**, **3h**, **3i**, and **5a**) compounds in the range of δ 7.656-6.960 confirms the presence of β-vinyl (=C-H) proton and another doublet at δ 7.206-6.707 confirms the presence of α-vinyl (=C-H) proton, respectively, confirming the formation of reported products. The global electrophilicity index (ω = 5.26 eV) shows that the (**3g**) molecule is a strong electrophile among all the studied compound. All compounds tend the formation of pyrazoline, oxazoline heterocyclic compounds which may have considerable pharmacological activities and material applications. The solvent-induced effects on the non-linear optical properties (NLO) were studied by using self-consistent reaction field (SCRF) method. As the solvent polarity increases, the β value have been found to increases monotonically. The compound (**3a**, **3c**, **3g**, **3h**, **3i**, and **5a**) displayed better non-linear optical (NLO) responses than the standard *p*-Nitro aniline (**pNA**) in solvent and as well as in gas phase. **3g** and **3i** have high NLO values even in gas phase which can be attributed to their unsymmetrical and high non-planar structure. All studied compounds (**3a**, **3c**, **3g**, **3h**, **3i**, and **5a**) show good antifungal and

antibacterial activity against *A. Niger* and gram-positive bacteria *B. subtilis* but **3g**, **3h**, and **3i** showed more prominent activity which can be attributed to their either substituents. Compounds **3h**, **3c**, **3a**, and **3g** showed better free radical scavenging than standard **BHT,** whereas **3h**, **3c**, **3a** showed better Fe^{2+} ion chelating activity than standard **EDTA,** and better Total reductive capability than standard **BHA.** Thus they are suitable for both material and biological applications.

Keywords: NMR, TD–DFT, NBO analysis, reactivity descriptor, NLO

* Corresponding author. e-mail: rnsvk.chemistry@gmail.com; Tel.: +919451308205

1. Introduction

Heterocyclic chemistry encompasses one of the largest divisions of chemistry, with important applications in biological [1], pharmaceutical [2], therapeutic [3], medicinal [4], catalytic [5], advanced materials [1-3] chemistry and the production of (non)-natural compounds [6]. The pyrrole moiety is one of the ubiquitous heterocyclic structures throughout both the plant and animal kingdoms [7]. The growing abundance of pyrrolic components in natural products, pharmaceuticals, and new materials lead the chemistry of pyrrole and its derivatives towards the center of interest. From the point of view of its intense utilization, the synthetic pyrrole chemistry has dominated. The chemistry of pyrroles is attracting steady attention because these heterocycles play an important role in nature and, at the same time, possess rich synthetic potential making them valuable synthons for the design of novel organometallic magnetic compounds or materials for optoelectronics [8], light-harvesting systems and photosensitizers for photodynamic cancer diagnostics and therapy [9], conducting organic polymers, pesticides. Pyrrole is also widely known as a biologically active scaffold which possesses a diverse nature of activities.

Scientific investigations on the bioavailability of chalcones from food sources are limited, but varieties of synthetic chalcones have been reported to possess a wide range of pharmaceutically important biological activities [10]. The chalcones have shown a wide range of biological activities [11] depending on the substitution pattern on the two aromatic rings around enone moiety. Several synthetic chalcones have been designed, synthesized, and have found numerous applications as pesticides; photo-protectors in plastics; solar creams, and food

additives [12]. In plants, chalcones are important intermediates in the biosynthesis of flavonoids and isoflavonoids [13]. Subsequently, they are precursors in the biosynthesis of a large number of flavonoid groups, including flavones, flavonols, dihydroflavonols, aurones, and isoflavones [14]. Chalcones constitute an important group of natural products that serve as precursors for the synthesis of various heterocyclic compounds like furans, pyrroles, pyrimidines, imidazoles, pyrazoles, 2-pyrazolines, and flavonoids [15-19]. Numerous studies dealing with chalcones have been carried out in the past few years [20-24]. Among many organic NLO materials, chalcone derivatives are noticeable materials for their excellent blue light transmittance [25] much better than those observed in inorganic crystals and show preference to crystallize as noncentrosymmetric structures. For this reason, they have been the objective of several experimental and theoretical studies, aimed mainly at the determination of their crystal structures [26]

On taking into account, the enormous areas of applicability of both types of moieties pyrrole and chalcone, it is a matter of great interest to have combined both. One of the rings of 1, 3-diaryl-2-propen-1-one skeleton is occupied by pyrrole derivatives, it generates Pyrrole-chalcone. In α, β-unsaturated carbonyl frame pyrrole moiety may have a position on β carbon or carbonyl carbon depends on reactants' functional during synthesis. Based on pyrrole position in α, β-unsaturated carbonyl frame two categories of chalcones are formed: (i) Pyrrole moiety attached to β carbon of α, β-unsaturated carbonyl frame of chalcone and (ii) Pyrrole moiety attached to the carbonyl carbon of α, β-unsaturated carbonyl frame of chalcone.

The combination of different pharmacophores in a pyrrole-chalcones has led to the formation of more active compounds. Pyrrole containing analogs are considered as a potential source of

biologically active compounds that contains a significant set of advantageous properties and can be found in many natural products. The marketed drugs containing a pyrrole ring system are known to have many biological properties such as antipsychotic, β-adrenergic antagonist, anxiolytic, anticancer (leukemia, lymphoma, and myelofibrosis, etc.), antibacterial, antifungal, antiprotozoal, antimalarial and many more. Due to the diversity of these analogs in the therapeutic response profile, many researchers have been working to explore this skeleton to its maximum potential against several diseases or disorders.

Ethyl 3,5–dimethyl–4-acetyl–1*H*–pyrrole–2–carboxylate (EDAPC) and Ethyl 3,5–dimetyl–4–formyl–1*H*–pyrrole–2–carboxylate (EDFPC) are found to be a suitable precursor for the synthesis of the pyrrole containing chalcones, however, biological and antioxidant activities of pyrrole-chalcones derived from these pyrrole precursors have not been yet studied and reported. Therefore, in present work biological and antioxidant activities of pyrrole-chalcones having different carbonyl positions with respect to pyrrole have been studied and the effect of others substituents have also been studied. Among the various properties of chemical compounds, biological activity plays a crucial role suggesting uses of the compounds in the medical applications.

2. Experimental Methodology

All the chemicals were used of an analytical grade. Ethyl 3,5–dimetyl–4–formyl–1H–pyrrole–2–carboxylate (EDFPC) **(1a)** and Ethyl 3,5–dimethyl-4-acetyl–1H–pyrrole–2–carboxylate (EDAPC) **(1b)** were prepared by an earlier reported method [27]. The ^{1}H NMR spectra of EDFPC and EDAPC were recorded in DMSO–d_6 on Bruker DRX–300 spectrometer using TMS

as an internal reference. The FT–IR spectra were recorded in KBr medium on a Bruker spectrometer. The UV–Visible absorption spectra of EDFPC and EDAPC, (1×10^{-5} M in DMSO) were recorded on V–670 JASCO spectrophotometer. The synthesis of all the synthesized compounds has been given in the supplementary material.

2.1 Antimicrobial Screening

The synthesized compounds were evaluated for their *in vitro* antifungal and antibacterial activity using *A. Niger*, *B. subtilis* strain, respectively, in potato dextrose agar media (PDA). The composition for this Nutrient Agar Media (per liter) is as Potato (200), Agar-agar (20), and Dextrose (20) gm. The solution (2.5 ml) of a synthesized compound (different concentrations) and 50 ml of molten sterile nutrient PDA media (5%) was poured into sterilized glass petridishes. A control PDA plate was also prepared for the test to compare the effect of test samples and to nullify the effect of solvent. All these plates were kept for 24 hours in UV chamber so that the samples had sufficient time to diffuse over a considerable area of the plate. After solidification of the medium, these plates were freshly seeded with a small portion of the mycelium of fungus in the form of 0.5 mm discs, carefully over the center of each PDA plate with the help of a sterilized needle. The plates were kept in incubation at 25±1°C for 96 hours. Ethanol was used as a solvent to prepare a desired solution of the synthesized compounds initially and also to maintain proper control.

The antibacterial activity was performed by the agar diffusion method at the concentration level of 200µg/ml and 100µg/ml. The agar media were inoculated with 1.0 ml of liquid cultures containing 10^5 microorganisms/ml. Diffusion time was 24 hours at 5^oC for all bacteria, and

incubation time was 12 hours at 30^{o}C. DMSO was used as solvent control. Inhibitory activity was measured (in mm) as the diameter of the observed inhibition zones.

2.2 Antioxidant activity

2.2.1 Free radical scavenging activity by DPPH method: Free radical scavenging capacities of synthesized compounds were determined according to the reported procedure [28]. The different concentrations (25-100 µg/mL) of newly synthesized compounds were added to each test tube and volume was made up to 4 ml using methanol and 3 ml of 0.004% DPPH in methanol was added. The mixtures were kept for incubated at room temperature under the dark condition for 30 min. The absorbance was recorded at 517 nm using UV-Visible spectrophotometer (Shimadzu UV-1800, Japan) and butylated hydroxyl toluene (BHT), was used as a reference. A control sample was prepared using the same volume without any compound and BHT, 95% methanol served as blank. The test was performed in triplicate and the results were averaged. Radical scavenging activity was calculated using the formula:

$$\textbf{\% of radical scavenging activity} = [(A_{control} - A_{test})/A] \times 100$$

Where $A_{control}$ is the absorbance of the control sample (DPPH solution without test sample) and A_{test} is the absorbance of the test sample (DPPH solution+test compound).

2.2.2 Iron chelating ability: The chelating effect was determined according to the literature method [29]. The test solution (2 ml) of different concentrations (25-100 µg/mL) in methanol was added to a solution of 2mM $FeCl_2$ (0.05 ml), the reaction was initiated by adding 5 mM ferrozine (0.2 ml) and total volume was adjusted to 5 ml with methanol. Then, the mixture was shaken vigorously and left at room temperature for 10 min. Absorbance of the solution was

measured spectrophotometrically at 562 nm. EDTA was used as a standard. The inhibition percentage of ferrozine-Fe complex formations was calculated using the formula:

$$\textbf{Metal chelating effect (\%)}=[(A_{control}-A_{sample})/A_{control}] \times 100$$

Where $A_{control}$ is the absorbance of control and A_{sample} is the absorbance of test compounds. Ascorbic acid is used as a control. The test was performed in triplicate and the results were averaged.

2.2.3 Reducing power assay: Reducing power of the test samples was evaluated by following the literature method [30]. Various concentrations of test compounds were mixed thoroughly with a mixture of 2.5 ml of 0.2 mM phosphate buffer (pH 7.4) and 2.5 ml of potassium ferricyanide. The resulting mixture was incubated at 50°C for 20 min, followed by the addition of 2.5 ml of trichloroacetic acid (10% w/v) and the mixture was centrifuged at 3000 rpm for 10 min. The upper layer of the solution was collected and mixed with 2.5 ml distilled water and later with 0.5 ml of ferrous chloride (0.1% w/v). The absorbance was measured at 700 nm against a blank sample. An increase in the absorbance of the reaction mixture indicated a higher reducing power of the test compounds.

3. Computational methodology

After the establishment of the structure of the molecule with the help of FT-IR, 1H and 13C NMR, UV-Visible, and elemental analysis, the initial geometries were generated with the help of Chem-Draw and Chem-3D Ultra program. All the quantum chemical calculations have been carried out with Gaussian 09 program package [31] using DFT method, B3LYP functional, and 6–311+G(d,p) basis set. Frequency calculation was conducted at the same level to test the stability of molecular structures. DFT frequencies are known to be overestimated than the experimental frequencies; these discrepancies were corrected directly scaling the calculated

wavenumbers with proper scaling factor [32]. The electronic transitions of the product were calculated using time dependent density functional (TD–DFT) theory which has emerged as a reliable standard tool for the theoretical treatment of electronic excitation spectra and recent works demonstrate the good accuracy for a wide range of systems [33]. Visualization of molecule, molecular orbital, and molecular electrostatic potential surfaces (MEPS) was performed with Gauss View program package [34]. QTAIM analysis has been found to be successful in the evaluation of associations, the existence of the hydrogen bonding and other weaker interactions, change of electronic properties in the formation of hydrogen bonds, red or blue shift in FT-IR spectrum, molecular geometry-distant consequences of H-bonding, π-electron delocalization shaping the H-bonding feature. The advantage of the QTAIM theory is that one can obtain information on changes in the electron density distribution as a result of either bond formation or complexes formation [35]. All QTAIM calculations were performed with the help of AIMALL program package [36]. The chemical reactivity and site selectivity of the molecular systems have been determined on the basis of Koopman's theorem [37]. Basis set superposition error (BSSE) was corrected by the counterpoise procedure of Boys and Bernardi [38], as ΔE (BSSE) = E (complex) – E (monomer Aunit) – E (Monomer Bunit). DFT derived global and local reactivity descriptors have been calculated using standard formula [39-45]. Global reactivity descriptors as electronegativity (χ) = –1/2(εLUMO + εHOMO), chemical potential (μ) = 1/2 (εLUMO + εHOMO), global hardness (η) = 1/2 (εLUMO – εHOMO), global softness (S) = 1/2η and electrophilicity index (ω) = μ2/2η are highly successful in predicting global reactivity trends.

4. Result and Discussion

4.1 *Structure, conformations, QTAIM and Reactivity*

The Scheme 1 shows ten synthesized pyrrole-chalcones (**3a-i**, and **5b**). The spectroscopic, DFT, QTAIM and Chemical reactivity of **3b**, **3d**, **3e**, and **3f** compounds have been already published [41, 44, 45]. This manuscript present antimicrobial and antioxidants activity of **3b**, **3d**, **3e**, and **3f** compounds and compared with the studied molecules (**3a**, **3c**, **3g**, **3h**, **3i**) and (**5b**). The product (**3a**, **3c**, **3g**, **3h**, **3i**) and (**5b**) is depicted in Scheme 1.

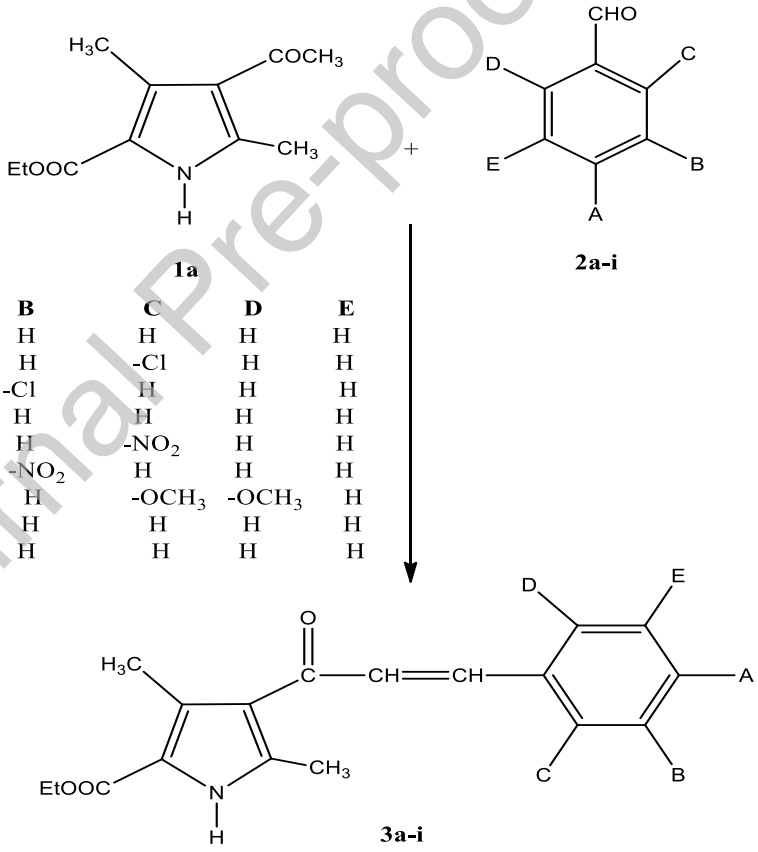

	A	B	C	D	E
3a	H	H	H	H	H
3b	H	H	-Cl	H	H
3c	H	-Cl	H	H	H
3d	-Cl	H	H	H	H
3e	H	H	$-NO_2$	H	H
3f	H	$-NO_2$	H	H	H
3g	H	H	$-OCH_3$	$-OCH_3$	H
3h	$-OCH_3$	H	H	H	H
3i	$-OCH_2C_6H_5$	H	H	H	H

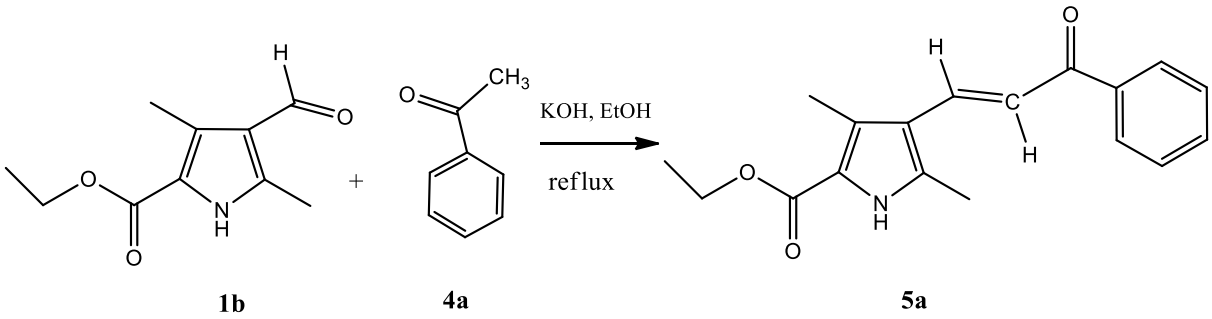

1b **4a** **5a**

Scheme 1. The route for the formation of compound (**3a-i**) and (**5a**)

The product Ethyl 3, 5-Dimethyl-4-(3-oxo-3-phenyl-propenyl)-1H-pyrrole-2-carboxylate (**3a**), (E)–ethyl 4–(3–(3–chlorophenyl)acryloyl)–3,5–dimethyl–1H–pyrrole–2–carboxylate**(3c)**, (E)–ethyl 4–(3–(2,6–dimethoxyphenyl)acryloyl)–3,5–dimethyl–1H–pyrrole–2–carboxylate **(3g)**, (E)–ethyl 4–(3–(3–methoxyphenyl)acryloyl)–3,5–dimethyl–1H–pyrrole–2–carboxylate **(3h)** and (E)–ethyl4–(3–(4–(benzyloxy)phenyl)acryloyl)–3,5–dimethyl–1H–pyrrole–2–carboxylate **(3i)** differ from Ethyl 3, 5-dimethyl-4-(3-phenyl-acryloyl)-1H-pyrrole-2-carboxylate (**5a**) in the position of pyrrole substitution around enone –C(=O)CH=CH- (α, β-unsaturated carbonyl) framework. All products have been obtained by the Claisen-Schmidt condensation of substituted pyrrole methyl ketone with benzaldehyde derivatives and substituted pyrrole aldehyde with benzene methyl ketones or acetophenone. The isomers of (**3a**, **3c**, **3g**, **3h**, **3i**) and (**5b**) show double bond exist in the *trans* configuration since the *cis* configuration is unstable due to the strong steric effects between the pyrrole ring and the carbonyl group. According to our calculation, the *trans* configuration is indeed more stable than the *cis* one. Thus, only the *trans* configuration was considered in this study. There are different conformers for the *trans* configuration of the studied molecules (**3a**, **3c**, **3g**, **3h**, **3i**) and (**5b**) as shown in Figure 1. The Potential energy surface scans, studies have been performed to understand the conformers' stability in (**3a**, **3c**, **3g**, **3h**, **3i**) and (**5b**). The potential energy curve is obtained as a function of

the dihedral angle around the C5-C4-C6-C15, C5-C4-C7-C15, C5-C4-C7-C15, C5-C4-C7-C15, C5-C4-C7-C15 bond by scanning it in steps of 10°, starting from the 0° value in (**3a**, **3c**, **3g**, **3h**, **3i**) and (**5b**), respectively. The **3a$_I$**, **3c$_I$**, **3g$_I$**, **3h$_I$**, **3i$_I$**, and **5a$_I$** conformers are of lower energy.

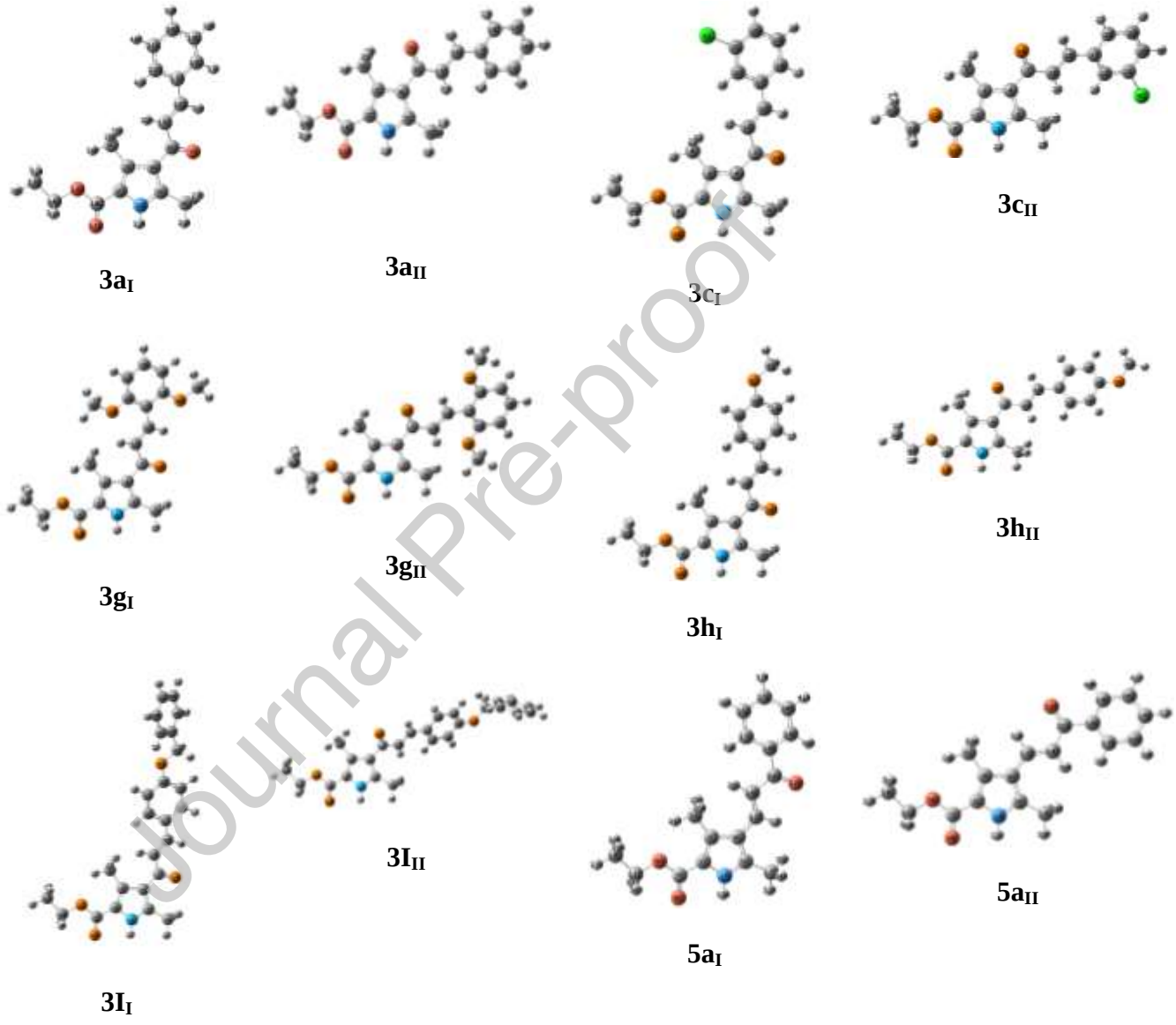

Figure 1. The conformers of (**3a-i**) and (**5a**) compound.

The enthalpy difference between **$3a_I$ / $3a_{II}$**, **$3c_I$ / $3c_{II}$**, **$3g_I$ / $3g_{II}$**, **$3h_I$ / $3h_{II}$**, **$3i_I$ / $3i_{II}$** and **$5a_I$ / $5a_{II}$** conformers calculated as -0.5251, -0.6152, -0.9465, -0.8703, -0.5183 and 0.2887 kcal /mol, respectively. The geometrical parameters of **3a, 3c, 3g, 3h, 3i,** and **5b** are listed in *supplementary material Table S1, S2, S3, S4, S5,* and *S6*, respectively. From torsion angle data, it can be seen that the enone unit in (**3a**, **3c**, **3g**, **3h**, **3i**) and (**5b**) are essentially planar, with a C=C-C=O torsion angle of average -174.69-176.77°, respectively.

It has been seen in the literature that those compounds having methyl and ethyl ester group on α and α' position of pyrrole derivative have the tendency to form dimers [27, 40-45]. Both the pyrrolic N-H and ester C=O group, the role lies in molecular association for dimer formation. The conformer **$3a_I$**, **$3c_I$**, **$3g_I$**, **$3h_I$**, **$3i_I$**, and **$5a_I$** of (**3a**, **3c**, **3g**, **3h**, **3i**) and (**5b**), respectively, have found suitable geometry for dimer formation through intermolecular hydrogen bonding by pyrrolic N-H and ester C=O. The calculated molecular geometry of dimers (**3a**, **3c**, **3g**, **3h**, **3i**) and (**5b**) are shown in *supplementary material Figure S1*. The binding energy of dimers is found to be 13.89, 13.98, 26.07, 27.42, 13.81, and 14.68 kcal/mol of (**3a**, **3c**, **3g**, **3h**, **3i**) and (**5b**), respectively, as per DFT calculation. The binding energy of dimer formation after basis set superposition error (BSSE) correction via the standard counterpoise method [38] are found to be 9.09, 10.4, 10.99, 11.23, 10.89, 9.06 kcal/mol in case of (**3a**, **3c**, **3g**, **3h**, **3i**) and (**5b**), respectively.

The calculated molecular graphs of (**3a**, **3c**, **3g**, **3h**, **3i**) and (**5b**) dimers are shown in *Supplementary material Figure S2*. The calculated binding energy of (**3a**) and (**3b**) found to be 16.62, 16.84, 24.77, 15.12, 16.70, and 14.71 kcal/mol. The binding energy of (**3g**) dimer is higher than (**3a**, **3c**, **3h**, **3i,** and **5a**) due to the presence of weaker interactions. In (**3a**, **3c**, **3g**, **3h**, **3i,** and **5a**) is higher than (**5a**) due to the presence of the carbonyl group (interaction C6-O7-

--C9/ C60-O67-C59, C6 ---O14-C7 / C47 ---O55-C48, C8--- H35-C15 / C49 ---H76-C56, C6---O14-C7 / C51---O59-C52, C6--- O14-C7 / C61---O69-C62) near to the pyrrole ring provides extra stability to the dimer as compared to (**5a**).

The calculated global parameters are given in Table 1. The calculated value of electrophilic charge transfer (ECT = -0.3485 (**3a**), -0.2518 (**3b**) eV) indicates that, charge flow from EDAPC to benzaldehyde and EDFPC to acetophenone, respectively. Therefore, EDAPC and EDFPC as electron donor and benzaldehyde and acetophenone as the electron acceptor. The increased value of global electrophilicity ω reveals that (**3a**) molecule is more electrophilic.

Table 1. Calculated ε_{HOMO}, ε_{LUMO}, energy band gap ($\varepsilon_L - \varepsilon_H$), chemical potential ($\mu$), electronegativity ($\chi$), global hardness ($\eta$), global softness ($S$), global electrophilicity index (ω) for **(1a, 1b)**, (**2a, 2c, 2g, 2h, 2i** and **4a**), (**3a**, **3c**, **3g**, **3h**, **3i** and **5a**) and Elecrophilicity based charge transfer (ECT) for reactant system [(**1a, 1b**)↔(**2a, 2b**)].

	ε_H	ε_L	$\varepsilon_L - \varepsilon_H$	$\mu = -\chi$	η	S	ω	ECT
(1a)	-6.1609	-1.0163	5.1446	3.5886	2.5720	0.1943	2.5032	
(2b)	-6.9446	-1.7257	5.2189	4.3352	2.6094	0.1916	3.6010	-0.3485
(2c)	-7.129	-2.0433	5.0857	4.5861	2.5428	0.1966	4.1356	-0.4084
(2g)	-6.3783	-1.4011	4.9772	3.8897	2.4886	0.2009	3.0398	-0.1679
(2h)	-6.3098	-1.4944	4.8154	3.9021	2.4077	0.2076	3.1620	-0.2255
(2i)	-6.3294	-1.3714	4.9580	3.8504	2.4790	0.2016	2.9902	-0.1581
(3a)	-5.9329	-1.8373	4.0959	3.8849	2.0479	0.2441	3.6848	
(3c)	-6.0270	-2.0460	3.9810	4.0365	1.9905	0.2511	4.0927	
(3g)	-6.4540	-2.5780	3.8760	4.5160	1.9380	0.2579	5.2616	
(3h)	-5.5783	-1.4887	4.0896	3.5335	2.0448	0.2445	3.0530	
(3i)	-5.7035	-1.6631	4.0404	3.6833	2.0202	0.2475	3.3577	
(4a)	-6.0314	-0.8158	5.2156	3.4236	2.6078	0.1917	2.2473	-0.2518
(5b)	-6.7258	-1.4808	5.2450	4.1033	2.6225	0.1906	3.2102	
(6c)	-5.7432	-1.7220	4.0207	3.7328	2.0103	0.2487	3.4656	

ε_H, ε_L, $\varepsilon_L - \varepsilon_H$, χ, μ, η, ω (in eV) and S (in eV^{-1})

Electrostatic potential surfaces of (**3a**, **3c**, **3g, 3h**, **3i,** and **5a**) are shown in Figure 2 to understand the reactivity of the molecules and correlate with dipole moment, electronegativity, partial charges, and site of chemical reactivity of the molecule. In (**3a**, **3c**, **3g**, **3h**, **3i,** and **5a**), the nucleophilic region present is around ester carbonyl group and the electrophilic region around the hydrogen atom of pyrrole N-H. In (**3a**, **3c**, **3g**, **3h**, **3i**) dimer formation due to the charge transfer, the equalization of chemical potential and electronegativity take place from the most positive electrostatic potential region of hydrogen of pyrrole N-H and α-methyl to the most electronegative electrostatic potential region of ester carbonyl group C=O. Similar observations have been seen in the case of (**5a**).

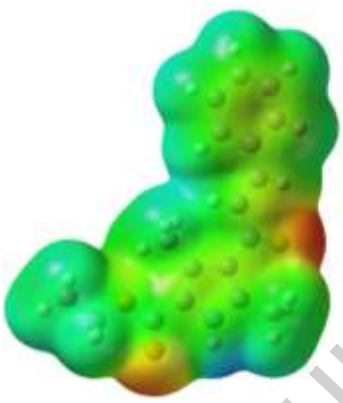

(3a)

(3c)

(3g)

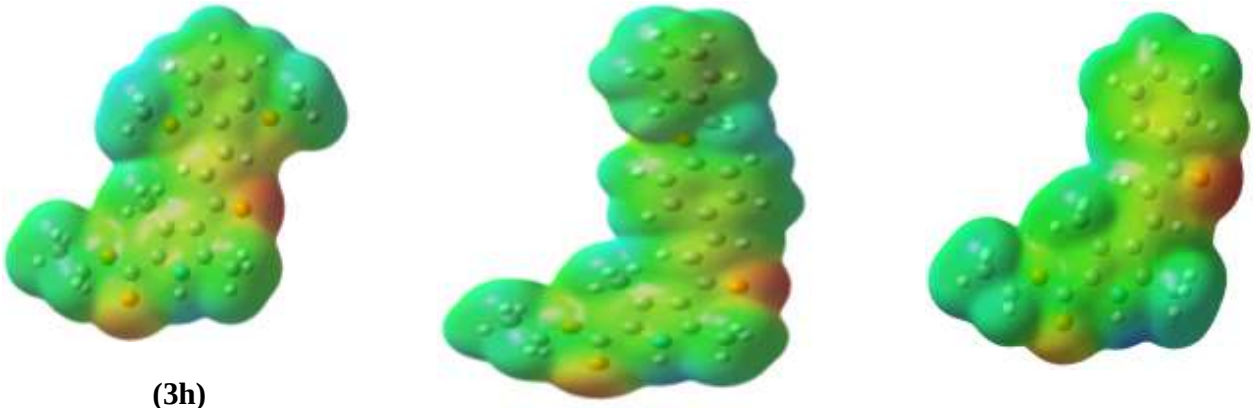

(3h) **(3i)** **(5a)**

Figure 2. The molecular electrostatic potential map of (**3a**, **3c**, **3g**, **3h**, **3i** and **5a**) of lower energy conformer.

4.2 Spectroscopic analysis

The structures of compounds have been established on the basis of spectral data. Detailed discussions of the spectral outcome for both compounds are described as follows. The simulated spectrum of FT-IR of (**3a**, **3c**, **3g**, **3h**, **3i**) and (**5a**) compounds are given in Figure 3. The calculated and experimental vibrational wavenumbers with assignment are given in Table 2.

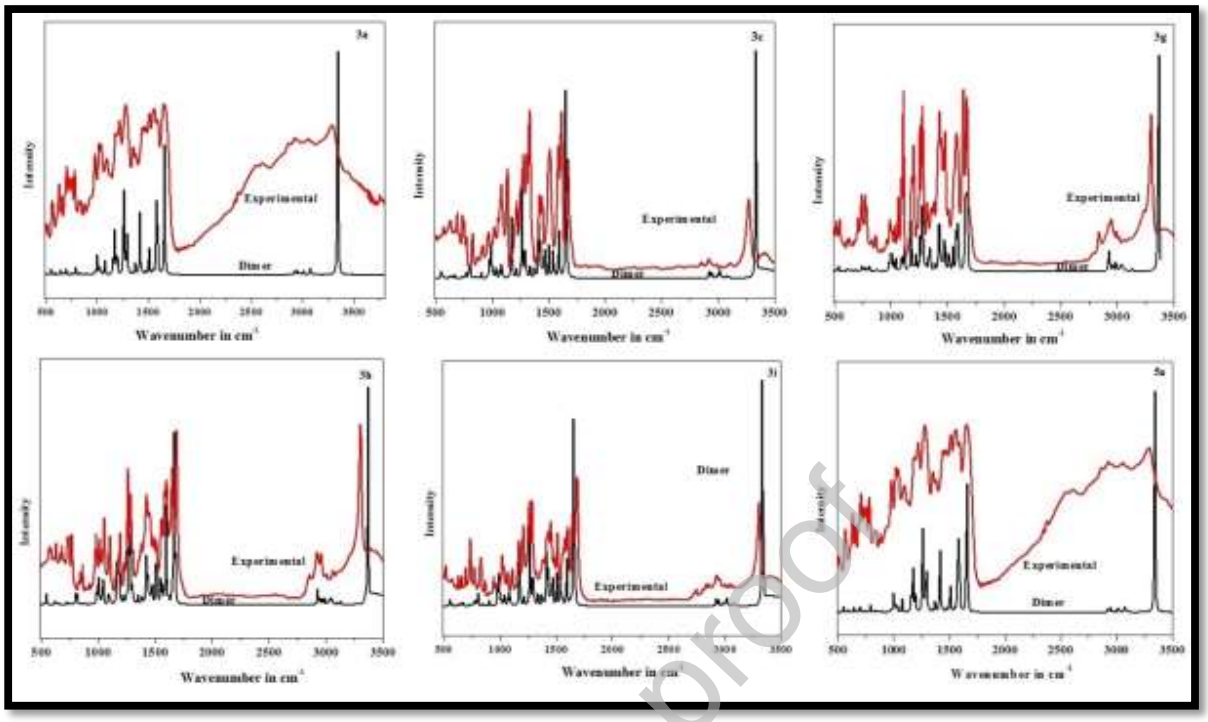

Figure 3. The FT-IR spectrum of (**3a**, **3c**, **3g**, **3h**, **3i** and **5a**) compounds of lower energy conformer

The N-H stretching generally seems in the region of 3500-3220 cm^{-1} and its accurate position generally depends upon the degree of hydrogen bonding as well as upon the degree physical state of the sample for frequency record. The experimental and calculated IR spectrum of (**3a**, **3c**, **3g**, **3h**, **3i,** and **5a**) shows N-H stretching vibration at 3340, (3355 (dimer), 3446 (monomer)), 3305, (3471 (dimer), 3639 (monomer)), 3290 (3474 (dimer), 3642 (monomer)), 3301 (3474 (dimer), 3641 (monomer)), 3306 (3473 (dimer), 3641 (monomer)), and 3312 (3292 (dimer), 3430 (monomer)), cm^{-1}, due to intermolecular hydrogen bonding, respectively. The calculated values of dimer corroborate well with the experimental values as compared to monomer. This observation correlates well with the reported literature involving intermolecular hydrogen bonded N–H system at 3358 cm^{-1} [46] and also with other pyrrole-chalcones and hydrazones derivatives [27, 33, 40-45]. The free ν_{NH} band reported in the literature (pyrrole-2-

carboxylic acid) at wavenumber 3465 cm^{-1} recorded in CCl_4 solution [46]. Therefore, we concluded that the solid-state IR spectrum of (**3a**, **3c**, **3g**, **3h**, **3i**) and (**5a**) indicates that all studied molecules exist in dimer form and the optimized geometry of dimer is shown in *Supplementary Figure S1*. The observed and calculated wagging mode of the N–H group appears at 789, 620, 630, 630, 628, 731 and 790, 694, 650, 745, 676, 742 cm^{-1} in (**3a**, **3c**, **3g**, **3h**, **3i**) and (**5a**), respectively, confirms the involvement of the pyrrolic N–H group in intermolecular attraction. The appearances of C=O stretching vibrations in (**3a**, **3c**, **3g**, **3h**, **3i**) and (**5a**) again indicate that studied molecules exist in dimer form in the solid-state. In (**3a**, **3c**, **3g**, **3h**, **3i**) and (**5a**) molecules ester carbonyl group stretching vibrations ($\nu_{C=O}$) are observed at 1676, 1687, 1670, 1686, 1684, 1653 cm^{-1}, and calculated as 1722, 1733, 1732, 1730, 1735 and 1688 cm^{-1}, respectively in dimer, and 1752, 1758, 1776, 1756, 1757 and 1691 cm^{-1} in monomer. This observed $\nu_{C=O}$ absorption band at 1676, 1687, 1670, 1686, 1684, 1653 cm^{-1} agrees well with the calculated wavenumber of the dimer as compared to the monomer in (**3a**, **3c**, **3g**, **3h**, **3i**) and (**5a**), respectively. This finding again closely correlates with the reported hydrogen bonded $\nu_{C=O}$ vibration at 1665 cm^{-1} for dimer of *syn*–pyrrole–2–carboxylic acid [46]. The vibrational frequencies of this mode again confirm carbonyl group (C=O) involvement in intermolecular hydrogen bonding. In the case of α-β unsaturated compounds the carbonyl stretching frequency shift away from the normal position due to the presence of strong electronegative substituent. The stretching vibration of the keto vinylic group ($\nu_{C=O}$) -CH=CH-CO- in **(3a, 3c, 3g, 3h, 3i)** calculated at 1649, 1657, 1714, 1720, 1716 cm^{-1} lower wavenumber than (**5a**) at 1760 cm^{-1}. The appended carbonyl group in α-β unsaturated framework of (**3a**, **3c**, **3g**, **3h**, **3i**) indicated that this forms a >C=O---C< interaction with that of methyl group present at α- position of pyrrole ring.

Table 2. Theoretical and Experimental (selected) vibrational wavenumbers of **(3a, 3c, 3g, 3h, 3i, and 5b)**, and their approximate assignments

Cal. (3a) Dimer	Exp.	Cal.(3c) Dimer	Exp.	Cal.(3g) Dimer	Exp.	Cal.(3h) Dimer	Exp.	Cal.(3i) Dimer	Exp.	Cal.(5b) Dimer	Exp.	Rep.	Assignments
3355	3340	3471	3305	3474	3290	3474	3301	3473	3306	3312	3292	3358	$\upsilon_{(N-H)}$-pyrrole
3094		3229	2936	3234	2994	3225	2957	3224	2926	3111		3020 - 2900	$\upsilon_{(C-H)}$-Vinylic
3069	3303	3225	2858	3329	2948	3195	2919	3328	2853	3061	3043	3100-2900	$\upsilon_{(C-H)}$-benzene
2940	2990	3141, 3133	2734	3110	2839	3132	2884	3195	2853 2744	2937	2927	2990-2850	$\upsilon_{(C-H)}$-ester Me +CH_2
1722	1676	1733	1687	1732	1670	1730	1686	1735	1684	1688	1653	1665	$\upsilon_{(C=O)}$ester
1649	1656	1657	1644	1714	1640	1720	1650	1716	1646	1760	1641	1633-1668	-CH=CH-CO- Keto vinylic group
1514	1552	1516	1608	1648	1578	1670	1599	1644	1601	1614	1565	1600	$\upsilon_{(C=C)}$-Benzene ring
-	-	-	-	-	-	-	-	1614	1574	-	-	1400-1600	$\upsilon_{(C=C)}$-Benzoxyl ring
1501	1445	1512	1418	1599	1505	1645	1510	1598	1510	1416	1439	1400-1540	$\upsilon_{(C=C)}$-keto vinylic group
1303	1297	1392	1295	1332	1429	1697	1427	1202	1429	1349	1349	1420-1360	$\upsilon_{(C=C)}$-pyrrole
1220		1011	948	1145	1198	1643	1192	1143	1166	1279	1279	1300-1000	δ_{ip} -(C-H) benzene
1097	1066	906	837	883	1180	1228	1103	873	1033	1205	1215	1300-1000	υ(C-O-C) ester
1025	1011	885	778	876	934	1045	981	843	990	1101	1093	1000-800	δoop(C-H)- Benzene
924		825	795	831	830	844	770	832	771	891	876	800-700	δoop(C-H)- Me
860		697	690	789	773	777	682	777	695	857	832	690	δoop(C=C)- Benzene ring
790	789	694	620	650	630	745	630	676	628	742	731	602	ω(N-H)-pyrrole

The experimental and calculated HC=CH stretching vibration in (**3a**, **3c**, **3g**, **3h**, **3i**) and (**5a**) appears at 1445, 1518, 1505, 1510, 1510, 1439 and 1501, 1512, 1599, 1645, 1598, 1416 cm^{-1} respectively, and assigned to the HC=CH stretching vibration of chalcone framework.

The ^{1}H NMR chemical shift values of **(3a, 3c, 3g, 3h, 3i)** and (**5a**) are given in *Supplementary Table S7*. The presence of a broad singlet at δ 9.033 (**3a**), 11.806 (**3c**), 11.575 (**3g**), 11.661 (**3h**), 11.871 (**3i**) 9.165 (**5a**) ppm corresponds to pyrrolic N-H. A multiplet of five protons of phenyl ring appears in the range δ 7.414-7.7.061 ppm (**3a**), 7.132-7.679 ppm (**3c**), δ7.531-7.559, 6.898-6.699, 6.844-6.860 ppm (**3g**), δ 7.426-7.482, 6.720-6.748 ppm (**3h**), δ. 7.681-7.709, 7.078-7.147, 6.939-7.049, 7.376-7.461 ppm (**3i**) and δ 7.792-7.192 ppm (**5a**) experimental spectrum. A detection of doublet in the experimental spectrum of (**3a**) at δ 7.656-7.602 (J=16.2 Hz), 7.735-7.762 (J=15.3 Hz) (**3c**), δ 7.211-7.263 (J=15.6 Hz) (**3g**), δ 7.862-7.915 (J=15.9 Hz) (**3h**), 7.835-7.888 (J=15.9 Hz) (**3i**), δ 6.998- 6.960 (J = 11.4 Hz) (**5a**) confirms the presence of β-vinyl (=C-H) proton and another doublet at δ 7.206-7.154 (J=16.2 Hz), (**3a**), δ 6.687-6.738 (J=15.3 Hz) (**3c**), δ 7.146-7.198 (J=15.6 Hz) (**3g**), δ 7.639-7.692 (J=15.9 Hz) (**3h**), δ 7.172-7.225 (J=15.9 Hz) (**3i**) δ 6.747-6.707 (J=12 Hz) (**5a**) confirms the presence of α-vinyl (=C-H) proton, respectively. The quartet observed at δ 4.367-4.344 (J = 6.9 Hz), 4.217-4.287, (J = 7.2 Hz), δ 4.258-4.325, (J = 6.6 Hz), 4.151-4.271, (J = 6.6 Hz), 4.255-4.321, (J = 6.6 Hz), 4.345-4.321 (J = 8 Hz), triplet at δ 1.414-1.367 (J = 7.1 Hz), δ 1.289-1.333 (J = 6.6 Hz), δ 1.233-1.280, (J = 6.3 Hz), δ 1.292-334 (J = 6.3 Hz), δ 1.446-1.490 (J = 6.3 Hz), δ 1.404-1.356 (J = 7.1 Hz) confirm the presence of methylene and methyl of ester group in the **(3a, 3c, 3g, 3h, 3i)** and (**5a**) molecule, respectively. The presence of singlets at δ 2.591, 2.523, δ 2.234, 2.434, δ 2.271, 2.390, δ 2.271, 2.353, δ 2.271, 2.351 ppm and 2.575, 2.527, confirm the presence of methyl group at α and β positions of **(3a, 3c, 3g, 3h, 3i)** and (**5a**).

4.3 *Linear and Nonlinear optical property*

Electronic absorption spectra of **(3a**, **3c**, **3g**, **3h**, **3i)** and (**5a**) show an intense lowest energy charge-transfer absorption band in the UV-visible region. The calculated electronic excitations of high oscillatory strength and experimental are listed in Table 3. The theoretical UV–Visible spectrum for **(3a, 3c, 3g, 3h, 3i)** and (**5a**) is shown in Figure 4.

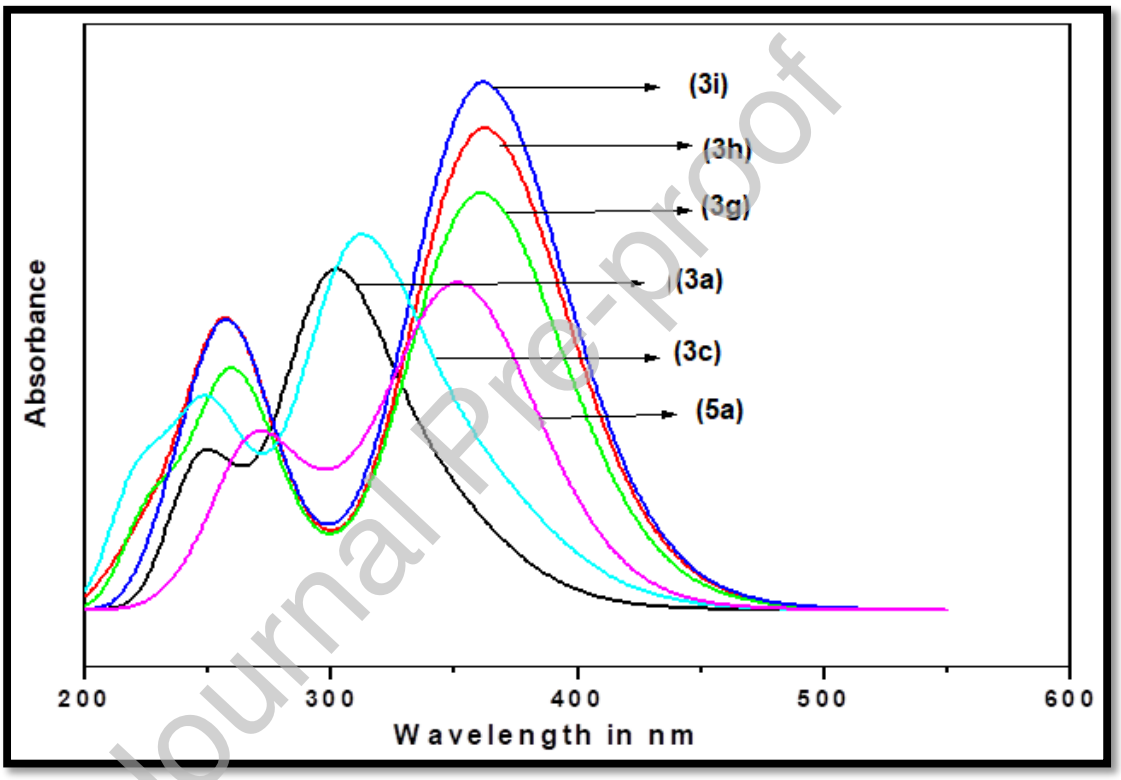

Figure 4. The Theoretical UV-Vis spectrum of (**3a**, **3c**, **3g**, **3h**, **3i,** and **5a**) compounds

The UV–Visible spectrum study reveals that the compound absorption is observed at 309, 249 (**3a**), 310, 245 (**3c**), 352, 242 (**3g**), 349, 244 (**3h**), 353, 249 (**3i**), 350, 240 (**5a**) nm in UV range as a result of π–π* transition.

Table 3. Calculated and experimental electronic excitations for (**3a**, **3c**, **3g**, **3h**, **3i** and **5a**): E / eV, oscillatory strength (f), (λ_{max} / nm) at TD–DFT/B3LYP/6–311+G(d,p) level.

S. No	Excitations	E (eV)	(f)	λ calcd.	λ Exp.	Assignment
			3a			
1	78 -> 80	3.9777	0.6979	311	309	π→π*
2	79 -> 81	5.0420	0.3853	253	249	n→π*
			3c			
1	86 -> 88	3.9670	0.7273	312.54	310	π→π*
2	87 -> 89	4.9063	0.3863	252.70	245	n→π*
			3g			
1	87 -> 88	3.3916	0.8811	365.89	352	π→π*
2	86 -> 89	4.7776	0.4757	259.51	242	n→π*
			3h			
1	95 -> 96	3.3921	0.6496	365.51	349	π→π*
2	94 -> 97	4.7691	0.4488	259.97	244	n→π*
			3i			
1	105 ->108	3.3897	0.9197	365.77	353	π→π*
2	106 ->109	4.7785	0.4739	259.46	249	n→π*
			5a			
1	79 -> 80	3.5067	0.6832	353.57	350	π→π*
2	79 -> 81	4.5694	0.1812	271.34	240	n→π*

Total static dipole moment (μ_0), mean polarizability ($|\alpha_0|$), anisotropy of polarizability ($\Delta\alpha$) and first hyperpolarizability (β_0), using x,y,z components are listed in Table 4. We have studied the solvent-induced effects on the dipole moment, polarizability, and non-linear optical properties (NLO) by using self-consistent reaction field (SCRF) method. Today computational calculation as an alternate choice provides extensive properties of materials, eg. hyperpolarizability which is a difficult task to measure directly [47]. Therefore, nowadays theoretical methods have been considered as useful techniques for prediction of polarizabilities and hyperpolarizabilities avoiding an expensive large amount of experimental synthetic work that precedes the measuring of NLO properties, which may not lead to the desired compound for practical applications. Total static dipole moment (μ_0), mean polarizability ($|\alpha_0|$), anisotropy

of polarizability ($\Delta\alpha$) and first hyperpolarizability (β_0), have been calculated by reporting literature methods [48].

The dipole moment in a molecule is an important property, which is mainly used to study the intermolecular interactions involving the nonbonded type dipole–dipole interactions, because the higher the dipole moment, the stronger the intermolecular interactions will be. The calculated dipole moment for (**3c**) (1.9385, 2.4776, 2.7575) molecule is lower than (**3a**) (2.146, 2.252, 2.446 D), (**3g**) (4.0842, 4.9932, 5.3373), (**3h**) (5.5814, 7.0277, 7.6641), (**3i**) (4.2309, 5.0652, 5.3872), (**5a**) (2.776, 3.336, 3.573), in vacuum, chloroform and methanol. Polarizability is an important electronic property, the calculated polarizability α_0, and the anisotropy of the polarizability $\Delta\alpha$ for **(3a**, **3c**, **3g**, **3h**, **3i)** and (**5a**) forms of still using B3LYP/6-311+G(d,p) in vacuum and solvent are listed in Table 4. The softness and polarizability are related to each other as "a soft species is also more polarizable." Thus, a hard (soft) species are known to correspond to a low (high) value of the polarizability as well as a small (large) size. The polarizability value of **(3a**, **3c**, **3g**, **3h**, **3i)** and (**5a**) increases monotonically as the solvent polarity increases. The compound (**3a**) is a hard species in comparison to (**3b**). Therefore, the polarizability of (**3b**) is higher. The first static hyperpolarizability (β_0) for compounds **(3a**, **3c**, **3g**, **3h**, **3i)** and (**5a**) increases with the polarity of the solvent and is better than standard para Nitro aniline (*p*–NA). Hence, the investigated molecule will show non–linear optical response and might be used as non–linear optical (NLO) material.

Table 4. Calculated Dipole moment (μ_0), Polarizability ($|\alpha_0|$), anisotropy of Polarizability ($\Delta\alpha$), First Hyperpolarizability (β_0) and their components for (**3a**, **3c**, **3g**, **3h**, **3i** and **5a**) compounds.

	B3LYP/6-311+G(d,p)			
	Dipole moment	**Polarizability**		**First hyperpolarizability**
	μ_0	$\|\alpha_0\|$	$\Delta\alpha$	β_0
3a	2.1466	28.8620	105.9135	8.0984
3c	1.9385	33.8419	115.9501	5.2470
3g	4.0842	35.1639	132.2266	33.6791
3h	5.5814	36.7125	127.8132	7.5079
3i	4.2309	30.7277	169.3611	41.5952
5a	2.7765	30.9897	105.4309	14.5947
	B3LYP/6-311+G(d,p) $CHCl_3$			
3a	2.2527	26.3461	125.6804	16.9891
3c	2.4776	41.5621	141.4556	13.3619
3g	4.9932	42.9021	160.8954	70.5265
3h	7.0277	44.9638	156.9115	21.4372
3i	5.0652	54.6171	194.0433	76.8431
5a	3.3361	38.0834	128.2914	32.4755
	B3LYP/6-311+G(d,p) MeOH			
3a	2.4466	28.2548	133.7775	21.1303
3c	2.7575	44.7474	151.4366	18.0572
3g	5.3373	46.1228	171.9840	73.0719
3h	7.6641	48.3512	168.5086	22.3735
3i	5.3872	58.4812	205.4506	94.8966
5a	3.5735	40.9316	137.1315	42.1254

μ_0 in Debye; $|\alpha_0|$ and $\Delta\alpha$ in 10-24 esu; β_0 in 10^{-30} esu,

4.4 Evaluation of Biological Activity

4.4.1 Evaluation of Antimicrobial activity

Living organisms provide material structures and environment for complicated chemistry of living. Chemical and physical reactions provide energy to maintain living functions and to renew structural material. Thus, consideration of biological properties is a natural extension of physical and chemical properties. Biological activity describes the beneficial or adverse effects of compounds on living matter. When a drug is a complex

chemical, this activity is exerted by the substance's pharmacophore but can be modified by the other constituents. Antifungal and antibacterial activity of study compounds **(3a-3i)** and (**5a**) were studied against *A. Niger* and human pathogenic gram-positive bacteria *B. subtilis*. All the synthesized compounds **(3a-3i)** and (**5a**) screened, exhibited remarkable *in vitro* activity against test organism strain. The bar diagram of inhibition of the zone for fungal and bacterial strain is shown in Figure 5 and 6, respectively and antifungal and antibacterial activity data reported in Table 5. The systematic perusal of antifungal activity with *A. Niger* found to be in *o*rder of **3h** >**3i** > **3g**>**3f** >**3e** > **3c** >**3b** > **3d** > **3a** >**5a**. Antibacterial activity against human pathogenic gram-positive bacteria *B. subtilis* found to be in *o*rder of 3h > 3g > 3i ≈ 3a > 3f > 3e >3b > 3c > 3d > 5a. A close inspection of screening data reveals that the directional position of the α, β-unsaturated group (-CH=CH-C=O) in chalcone and the nature of substitution at aromatic rings are highly influencing the antifungal activity of these compounds.

The pyrrole chalcones in which pyrrole is attached to carbonyl group have high antifungal activity than pyrrole is attached to unsaturated β carbon of group (-CH=CH-C=O). The ether substituents (**3h**, **3g** and **3i**) show good activity for both antifungal activity and antibacterial study relative to other substituents. Both donating and withdrawing groups are found to enhance the antifungal activity. Another observation noticed significantly from Table 5 is that degree of inhibition increases with the increasing concentration of testing these pyrrole chalcones.

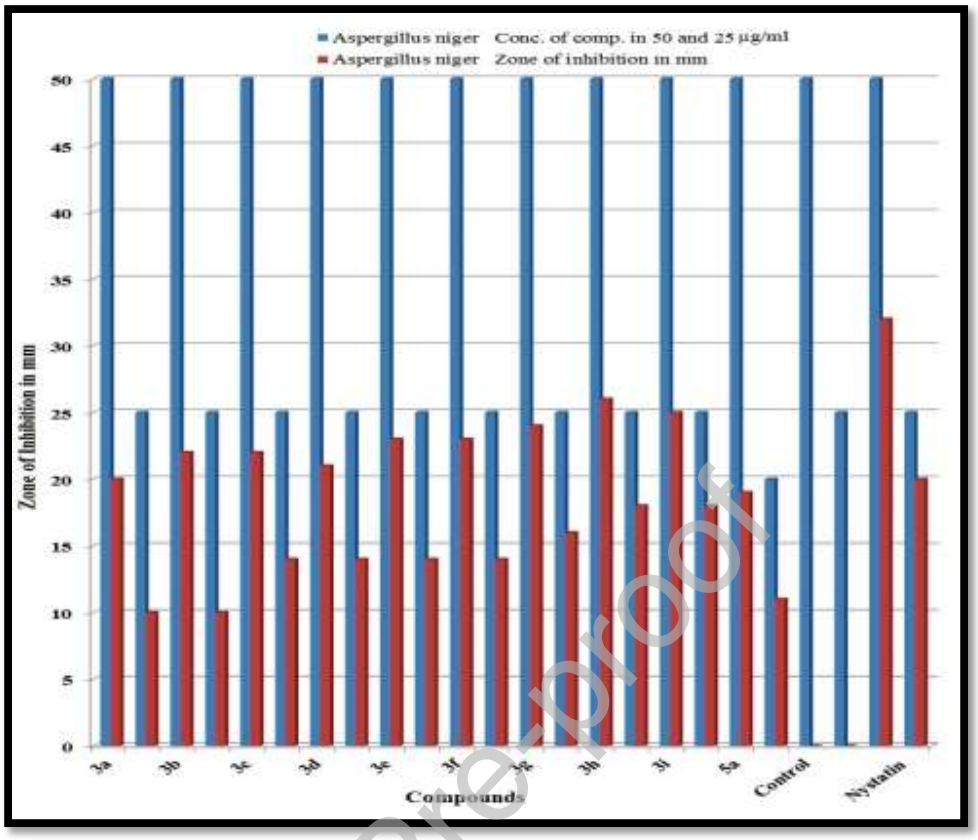

Figure 5. The bar diagram of antifungal activity of (**3a**, **3c**, **3g**, **3h**, **3i** and **5a**) compounds

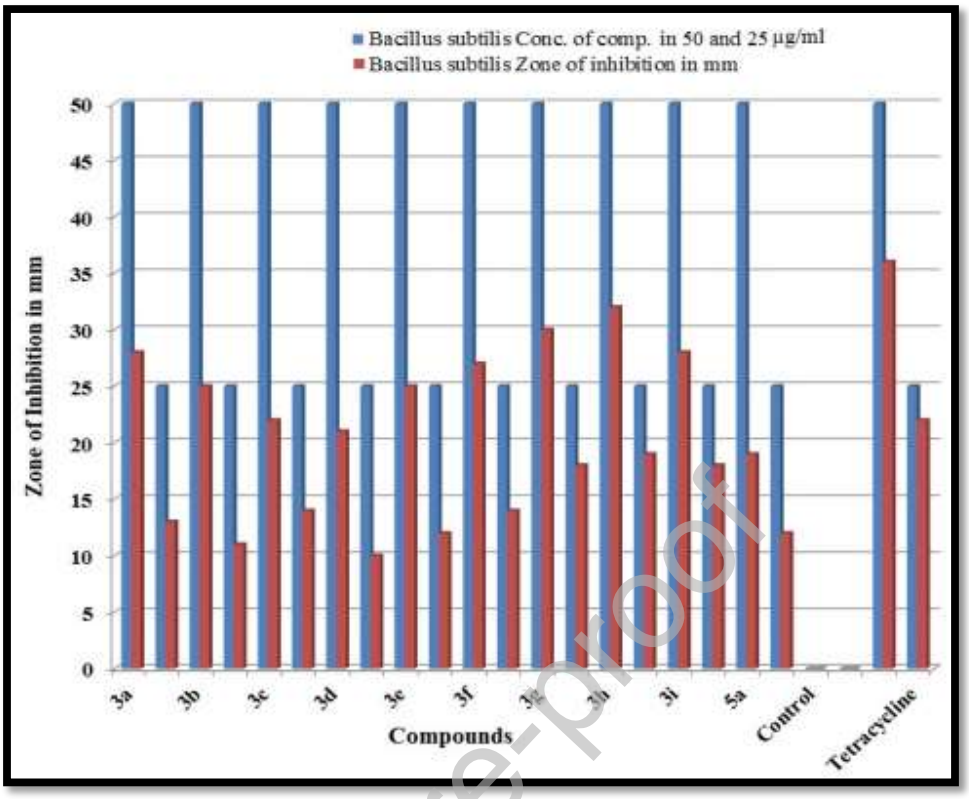

Figure 6. The bar diagram of antibacterial activity of (**3a**, **3c**, **3g**, **3h**, **3i** and **5a**) compounds

Table 5. Antimicrobial screening data against for study compounds

Comp	*Aspergillus niger*		*Bacillus subtilis*	
	Conc. of comp. in µg/ml	Zone of inhibition in mm	Conc. of comp. in µg/ml	Zone of inhibition in mm
3a	50	20	50	28
	25	10	25	13
3b	50	22	50	25
	25	10	25	11
3c	50	22	50	22
	25	14	25	14
3d	50	21	50	21
	25	14	25	10
3e	50	23	50	25
	25	14	25	12
3f	50	23	50	27
	25	14	25	14
3g	50	24	50	30

	25	16	25	18
3h	50	26	50	32
	25	18	25	19
3i	50	25	50	28
	25	18	25	18
5a	50	19	50	19
	20	11	25	12
Control	50	32	50	36
Nystatin / Tetracycline	25	20	25	22

4.4.2 Free radical scavenging activity by DPPH method: The graphical representation of free radical scavenging activity is given in Figure 7. All the synthesized compounds were screened for their free radical scavenging activity by DPPH method. The Freshly prepared solution exhibits a deep blue color with the absorption maximum at 517 mm. This deep blue color generally fades when the antioxidant is present in the solution. All compounds have exhibited varied free radical scavenging capacity by comparison with the standard Butylated hydroxy toluene (BHT) [49]. DPPH assay (IC50 µg/mL) value of DPPH radical scavenging of tested compounds (**3a-i** and **5a**) is reported in Table 6. The systematic of free radical scavenging activity with respect to standard BHT (48.63) for synthesized chalcones found to be in order of **3h** (38.12) > **3c** (43.38) > **3a** (44.58) > **3g** (45.58) > **3i** (50.03) > **5a** (52.55) >**3e** (62.63) >**3b** (75.58) > **3d** (82.56) > **3f** (87.41). Further, it was observed that the compound **3h** having orth-methoxy substituent has excellent activity with minimum IC_{50} value. The other compounds showed moderate to good activity. From the activity results it is revealed that among the tested compounds, compounds (**3h, 3c, 3a** and **3g**) displayed better free radical scavenging activity with least IC_{50} value than standard BHT.

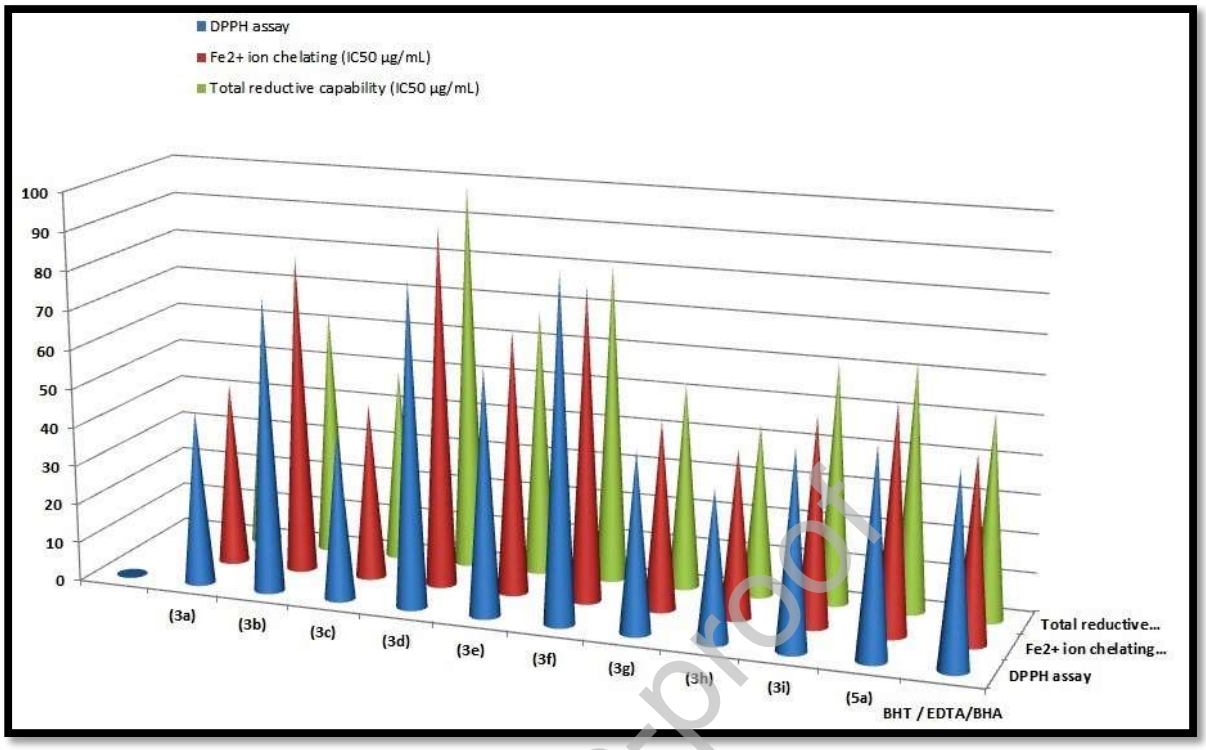

Figure 7. The bar diagram of Antioxidant Activity of (**3a**, **3c**, **3g**, **3h**, **3i** and **5a**) compounds

4.4.3 Iron chelating ability: The graphical representation of iron chelating ability is given in Figure 7. The iron chelating study measures the ability of antioxidants to compete with Ferrozine in chelating ferrous ion [50]. The Fe^{+2} chelating capacities varied significantly among different compounds. Fe^{2+} ion chelating (IC_{50} µg/mL) value of tested compounds (**3a-i** and **5a**) are reported in Table 6. The systematic of iron chelating ability with respect to standard EDTA (47.17) for synthesized chalcones have been in order of **3h** (42.67) >**3c** (45.01) >**3a** (47.02) >**3g** (48.02) >**3i** (52.88) >**5a** (57.89) >**3e** (67.34) >**3f** (79.89)>**3b** (81.69)>**3d** (91.88). From the activity results it is revealed that among the tested compounds, compounds (**3h, 3c** and **3a**) displayed better Fe^{2+} chelating capacities with least IC_{50} value than standard EDTA. The other compounds showed moderate to good activity.

Table 6. IC_{50} value of DPPH radical scavenging, Ferrous ion chelating and total reductive capability activity of test compounds (5a-k).

Test Compounds	DPPH assay (IC_{50} µg/mL)	Fe^{2+} ion chelating (IC_{50} µg/mL)	Total reductive capability (IC_{50} µg/mL)
(3a)	44.58	47.02	51.59
(3b)	75.58	81.69	63.13
(3c)	43.38	45.01	49.19
(3d)	82.56	91.88	98.98
(3e)	62.63	67.34	68.03
(3f)	87.41	79.89	81.24
(3g)	45.58	48.02	52.59
(3h)	38.12	42.67	44.04
(3i)	50.03	52.88	61.25
(5a)	52.55	57.89	63.12
BHT / EDTA/BHA	48.63	47.17	52.30

Butylated hydroxy toluene (BHT) used as standard for DPPH radical scavenging activity;
Ethylenediaminetetraacetic acid (EDTA) is used as a standard for Fe^{2+} ion chelating activity;
Butylated hydroxyanisole (BHA) used as standard for total reductive capability.

4.4.4 Total reductive capability: The graphical representation of total reductive capability is given in Figure 7. The reduction of Fe^{3+} to Fe^{2+} is often used as an indicator of electron-donating activity, which is an important mechanism of phenolic antioxidant action. In the reducing power assay, the presence of antioxidants in the synthesized compounds would result in the reduction of Fe^{+3} to Fe^{+2} by donating electron(s). The amount of Fe^{+2} complexes was then monitored by measuring the formation of Perl's Prussian blue at 700 nm. Absorbance at 700 nm indicates an increase in reducing ability [51]. Total reductive capability (IC_{50} µg/mL) values of tested compounds (**3a-i** and **5a**) are reported in Table 6. It was found that the reducing power of all the synthesized compounds increased with the increase in their concentrations. Total reductive capability of Fe^{3+} to Fe^{2+} (IC_{50} µg/mL) of tested compounds (**3a-i** and **5a**) with respect

to BHA (52.30) found to be in order of **3h** (44.04) > **3c** (49.19) >**3a** (51.59) >**3g** (52.59) >**3i** (61.25) >**5a** (63.12) > **3b** > (63.13) > **3e** (68.03) >**3f** (81.24) > **3d** (98.98). Compounds (**3h, 3c** and **3a**) displayed better reducing power with least IC_{50} value than standard Butylated hydroxyanisole (BHA). The other compounds showed moderate to good activity.

5. Conclusions

The studied compounds **(3a**, **3c**, **3g**, **3h**, **3i)** and (**5a**) have been synthesized and characterized by experimental techniques and theoretical calculations. The effect of carbonyl group position in the enone unit (C=C-C=O) of pyrrole chalcone have been clearly seen in spectroscopy and DFT calculations. The detailed spectroscopic, DFT, and antimicrobial analysis have been performed and the results will compare with the experimental data. The presence of doublet in ^{1}H NMR spectra of **(3a**, **3c**, **3g**, **3h**, **3i)** and (**5a**) compounds suggested β-vinyl (=C-H) proton and α-vinyl (=C-H) proton which confirms the formation of the product. The electronic absorption bands in **(3a**, **3c**, **3g**, **3h**, **3i)** and (**5a**) have been assigned by TD-DFT method and found to be n→π* and π→π* in nature. The global electrophilicity index (ω = 5.26 eV) shows that the (**3g**) molecule is a strong electrophile than all studied molecules. The synthesized compounds favor the formation of pyrazoline, oxazoline heterocyclic compounds which may have considerable pharmacological activities and material applications. The solvent-induced effects on the non-linear optical properties (NLO) were studied by using self-consistent reaction field (SCRF) method. As the solvent polarity increases, the *β* value increases monotonically. The compound **(3a**, **3c**, **3g**, **3h**, **3i)** and (**5a**) displayed better non-linear optical (NLO) responses than the standard *p*-nitroaniline (**pNA**) in solvent and as well as in gas phase. The studied compounds (**3a**, **3c**, **3g**, **3h**, **3i**, and **5a**) show good antifungal and antibacterial activity against *A. Niger* and

gram-positive bacteria *B. subtilis*. Studied compounds showed promising free radical scavenging and Fe^{+2} ion chelating activity.

Acknowledgment

The author is thankful to the NCERT and CSIR (No.:09/107(0379)/216-EMR-I) for financial support.

Credit Author Statement

- Conception or design of the work
- Data collection
- Data analysis and interpretation
- Drafting the article
- Critical revision of the article
- Final approval of the version to be published

Declaration of Interest Statement

We wish to confirm that there are no known conflicts of interest associated with this publication and there has been no significant financial support for this work that could have influenced its outcome.

Graphical abstract

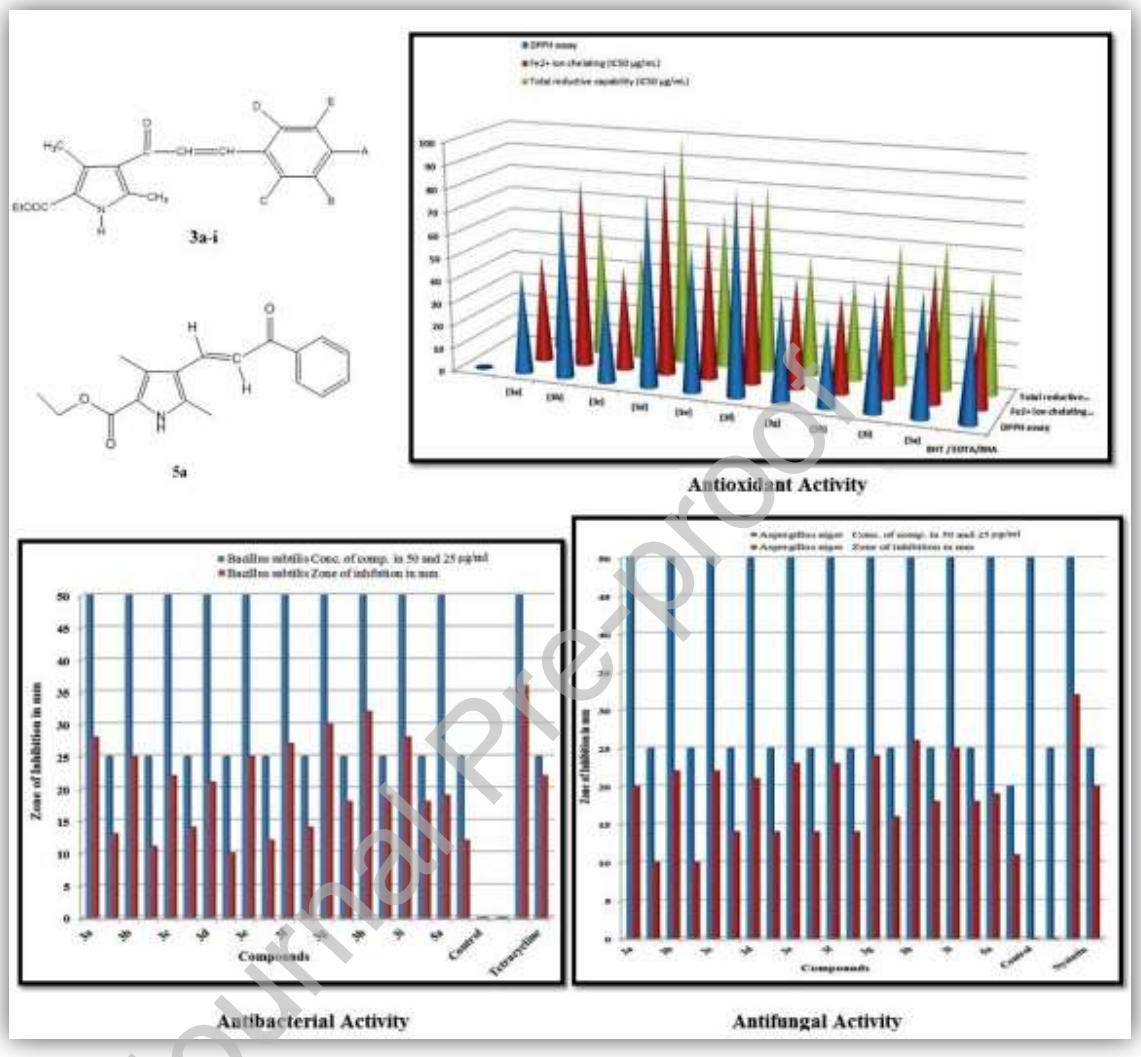

Reference

[1]. M. A. P. Martins, C. P Frizzo, D. N. Moreira, N. Zanatta, H.G. Bonacorso, Chem. Rev., 108(2008) 10933

[2] M. J. Riveira, A. La-Venia, M. P. Mischne, J. Org. Chem. 73(2008) 8678

[3] L. I. Vereschagin, F. A. Pokatilov, V. N. Kizhnyaev, Chem. Heterocycl. Compd. 44(2008) 1

[4] N. Isambert, R. Lavilla, Chem.–Eur. J. 14(2008) 8444

[5] F. E. Hahn, M. C. Jahnke, Angew. Chem., Int. Ed. 47(2008) 3122

[6] K. Dooleweerdt, T. Ruhland, T. Skrydstrup Org. Lett. 11(2009)221

[7] K. Fukamizu, Y. Miyake, Y. Nishibayashi, J. Am. Chem. Soc. 130(2008)10498

[8] R. T. Hayes, M. R. Wasielewski, D. Gosztola, J. Am. Chem. Soc. 122(2008)5563

[9] J. Rimarčik, V. Lukeš, E. Klein, M. Griesser, A. Kelterer chem. Phys. 353(2008) 177

[10] XL. Liu, Y. J. Xu, M. L. Go Eur. J. Med. Chem. 43(2008) 1681

[11] R. Gacche, M. Khsirsagar, S. Kamble, B. Bandgar, N. Dhole, K. Shisode, A. Chaudhari, Chem. Pharm. Bull. 56(2008)897

[12] R. J. Hsieh, J. E. Kinsella, Adv. Food Nutr. Res. 33(1989) 233

[13] J. P. Strachan, , D. F. O'Shea, T. Balasubramanian, J. S. Lindsey, J. Org. Chem. 65(2000) 3160

[14] J. B. Harborne, T. J. Mabry, H. Mabry, (1975) The Flavonoids, Chapman and Hall: London.

[15] A. E. Mattson, A. R. Bharadwaj, A. M. Zuhl, K. A. Scheidt, J. Org. Chem, 71(2206) 5715

[16] A. Tafi, R. Costi, M. Botta, R. Di Santo, F. Corelli, S. Massa, S, Ciacci, F. Manetti, M. Artico, J. Med. Chem. 45(2002) 2720

[17] B. A. Bhat, K. L. Dhar, S. C. Puri, A. K. Saxena, M. Shanmugavel, G. N. Qazi, Bioorg. Med. Chem. Lett. 15(2005) 3177

[18] D. Azarifar, H. Ghasemnejad, Molecule 8(2003) 642

[19] K. M. Lakshmi, P. B. Veda, R. Venkat, Synth. Commun. 35(2005) 1971

[20] D. Millán, M. Domínguez, M. C. Rezende, Dyes and Pigments 77(2008) 441

[21] B. Gu, W. Ji, P. S. Patil, PS, Dharmaprakash, SM, J. Appl. Phys. 103(2008) 103511

[22] L. Mager, C. Melzer, M. Barzoukas, A. Fort, S. Mery, J. F. Nicoud, Appl. Phys. Lett. 71(1997) 2248

[23] M. P. Cockerham, C. C. Frazier, S. Guha, E. A. Chauchard, Appl. Phys. B 53(1991) 275

[24] H. Forejtníková, K. Lunerová, R. Kubínová, D. Jankovská, R. Marek, R. Kareš, V. J. Suchý, Vondráček, M Machala, Toxicology 208(2005) 81

[25] W. Tam, B. Gucrim, J, C. Calabreso, S. U. Sterenson, Chem Phys. Lett. 1540(1989) 93.

[26] V. Shettigara, P. S. Patila, S. Naveenb, S. M. Dharmaprakasha, M. A. Sridharb, J. S. Prasad, Journal of Crystal Growth 295(2006)44

[27] P. Rawat, R. N. Singh J. Mol. Struct. 1075(2014) 462

[28] Md. M. Rahman, Md. B. Islam, M. Biswas, A. H. M. Khurshid Alam B. M. C. Res Notes 8 (2015)621

[29] M. S. Blois, Nature. 181(1958)1199.

[30] R. Nayan, B. Bhalodia, B. Pankaj R. N. Nariya, V. J. Acharya, A. Shukla 2013 Apr-Jun; 34(2): 209

[31] M. J. Frisch et-al, , Gaussian 09, Revision B01; Gaussian: Wallingford CT 06492, 2010.

[32] M P Anderson , P Uvdal, J Phys Chem A 109(2005) 2937

[33] P. Rawat, R. N. Singh, Spectrochimica Acta Part A 140(2015) 344

[34] R. Dennington, T. A. Keith, J. M. Millam, K. S. Mission, GaussView, Version 6.1, 2016

[35] R.F.W. Bader, Atoms in Molecules: A Quantum Theory; Clarendon Press, Oxford, 1990

[36] A. Todd, T. K. Keith, Gristmill Software, Overland Park KS, USA, AIMAll (Version 19.10.12), 2019

[37] T. Tsuneda, J. W. Song, S. Suzuki, K. Hirao The Journal of Chemical Physics 133(17) 174101

[38] S. F. Boys, F Barnardi, Mol. Phys 19(1990) 553

[39] P. Rawat, R. N. Singh, Arabian J. Chem. 12(2019) 1219

[40] P. Rawat, R. N. Singh, J. Mol. Struct. 1074(2014) 201

[41] R. N. Singh, V. Baboo, P. Rawat, A. Kumar, D. Verma, Spectrochimica Acta Part A 94(2012) 288

[42] R. N. Singh, P. Rawat, S. Sahu, J. Mol. Struct, 1076(2014) 437

[43] R. N. Singh, P. Rawat, S. Sahu, J. Mol. Struct, 1065(2014) 99

[44] R. N. Singh, V. Baboo, P. Rawat, V.P. Gupta, J. Mol. Struct, 1037(2013) 338

[45] R. N. Singh, P. Rawat, V. Baboo, Y. Kumar, J. Mol. Struct, 1085(2015) 258

[46] A. T. Dubis, , S. J. Grabowski, , D. B. Romanowska, T. Misiaszek, J. Leszczynski, J. Phys. Chem. A 106(2002) 10613

[47] A. E De, A. Machado, L. A. De Souza, H. F. Dos Santos, B. Wagner J. Polymer Sci. Part B: Polymer Phys. 49(2011) 1410

[48] J. N. Woodford, C. M. Pauley, A. H. Wang, J. Phys. Chem. A, 101(1997) 1989

[49] O. J. Olorunjuwon,, M. A Gbadegesin, O. A Odunola, Pharmacognosy Res. 7(2015) 49

[50] R. Sudan, M Bhagat, S. Gupta, J. Singh, A Koul, BioMed Res. Internat. (2014) 1

[51] M. Rahman, M. Islam, K. Biswas, B. M. C. Res. Notes, 8(2015) 621